Shaping the Global High-Resolution TanDEM-X Digital Elevation Model

Martin Huber [ORCID], Nicole Osterkamp, Ursula Marschalk, Raphael Tubbesing,
Anna Wendleder, Birgit Wessel [ORCID], and Achim Roth [ORCID]

Abstract—The global digital elevation model (DEM) produced by the TanDEM-X (TerraSAR-X add-on for digital elevation measurements) mission is an interferometric elevation model with unprecedented quality, accuracy, and coverage. It represents an unedited surface model as artifacts inherent to the interferometric synthetic aperture radar acquisition and processing technique are still present. The most prominent artifacts in the DEM are water bodies appearing with a rough surface due to low coherence. Additionally, outliers, voids, and larger data gaps may be present in this dataset. Therefore, DEM editing is crucial for many applications including hydrology or orthorectification of remote sensing data. Depending on the field of application, different techniques of quality enhancement are required. This article provides a comprehensive description of a semi-automatic framework specially developed for generating an edited version of the TanDEM-X dataset by shaping the high-resolution 12 m DEM with focus on water areas, outlier handling, and void filling. The default configuration parameters of the workflow can thereby be adapted interactively for challenging areas where appropriate. A quality assessment of the resulting edited DEM was done by statistical measures, visual methods, as well as by an artifact evaluation.

Index Terms—Digital elevation model (DEM), editing, filtering, flood modeling, hydrology, interferometry, quality assessment, remote sensing, synthetic aperture radar (SAR).

I. INTRODUCTION

DIGITAL ELEVATION models (DEMs) are numerical representations of the Earth surface. They are an essential source of topographic information for various applications including hydrology, hydrodynamics, and flood inundation modeling [1]–[5], geomorphology and geomorphometry [6]–[9], as well as forest mapping [10]–[12]. The geometric and radiometric corrections of digital satellite data [13]–[17] benefit from a precise description of the Earth's relief.

The DEM of the German satellite mission TanDEM-X (TerraSAR-X Add-on for digital elevation measurements) is

Martin Huber, Ursula Marschalk, Anna Wendleder, Birgit Wessel, and Achim Roth are with the German Remote Sensing Data Center, German Aerospace Center, 82234 Oberpfaffenhofen, Germany (e-mail: martin.huber@dlr.de; ursula.marschalk@dlr.de; anna.wendleder@dlr.de; birgit.wessel@dlr.de; achim.roth@dlr.de).

Nicole Osterkamp and Raphael Tubbesing are with the Company for Remote Sensing and Environmental, 81243 München, Germany (e-mail: nicole.osterkamp@dlr.de; raphael.tubbesing@dlr.de).

currently one of the most accurate global DEMs [18]. The mission was realized by a cooperation between the German Aerospace Center (DLR) and Airbus Defence and Space. DLR's responsibility comprises the generation of the TanDEM-X DEM, the science coordination, and the provision of products for research purposes. Airbus Defence and Space, being responsible for the commercial exploitation, applied further processing to the TanDEM-X DEM dataset resulting in the WorldDEM^TM product [19].

The twin satellites TerraSAR-X and TanDEM-X are flying in a close helix formation with distances between 300 and 500 m [20]. This enables the derivation of height information by applying single pass synthetic aperture radar (SAR) interferometry. The SAR image pairs were acquired between December 2010 and January 2015 in StripMap mode with horizontal transmit and receive polarization. The TanDEM-X DEM has a 12 m spatial resolution with specified 10 m absolute height accuracy [90% linear error (LE90)] and 2–4 m relative accuracy depending on the terrain slope [20], [21]. The accuracy of the TanDEM-X DEM has been ensured by an intensive calibration and validation procedure [22], [23], mainly based on ground control points from Ice, Cloud, and Land Elevation Satellite [24], [25]. Furthermore, Wessel *et al.* [26] compared the TanDEM-X DEM with kinematic global positioning system point reference datasets, where the mean error (ME) is −0.17 m with a root mean square error (RMSE) of 1.29 m.

The TanDEM-X DEM is an interferometric surface model where no additional editing was performed. Consequently, artifacts inherent to the interferometric SAR (InSAR) acquisition and processing technique are still present. Smooth water bodies appear as rough surfaces in the DEM due to two effects causing high noise: specular reflection leads to low backscatter and temporal decorrelation of the phase induces a loss of coherence. This also affects bistatic systems like TanDEM-X. The helix formation leads to a small along-track distance between the two satellites. The time difference of even a few milliseconds between the acquisitions results in a decorrelation of the backscattered signals over water and therewith the interferometric phase is random [27], [28]. Suchandt *et al.* [29] describe along-track applications, processing, and effects with the bistatic SRTM/X-SAR (shuttle radar topography mission). As the phase is transformed into the elevation value, this noise leads to significant height changes from pixel to pixel. Such higher variation of elevation values can also appear whenever the coherence is low [30],

[31], e.g., due to high but varying vegetation like loose forest stands. Nevertheless, low coherence and low backscatter serve as main indicators to identify rivers and lakes. A reliable automatic detection of open water in InSAR DEMs is still limited as, e.g., the appearance of wet snow areas or radar shadow fulfill these criteria, too. The SRTM as well as Airbus Defence and Space for the WorldDEM^TM product solved this by a substantial manual procedure [19], [32]. Moreover, outliers, void DEM values, and bigger data gaps are present. Outliers are local and occur either as spikes (positive) or troughs (negative). They can easily be detected by analyzing the local statistics of the surroundings. Voids appear whenever no information could be obtained during the SAR imaging for a specific area—e.g., due to layover or radar shadow—that could not be filled by another TanDEM-X image strip. In a few cases, planned acquisitions could not be executed during the mission's imaging period (December 2010 to January 2015), either due to imaging conflicts or failures during the data download. Such outages led to even bigger data gaps. Commonly, other globally available DEM data such as SRTM DEM or the Advanced Spaceborne Thermal Emission and Reflection Radiometer Global DEM (ASTER GDEM) are used as infill [19], [33]. These datasets are also used in our approach to fill larger void areas in the TanDEM-X DEM.

Random noise in a DEM perturbs the derivation of terrain parameters like slope and flow direction. It can also affect geometric processing like the orthorectification of SAR images. Here, the imaging geometry is reconstructed for every pixel and rapid variation of higher and lower elevation values over actually flat areas leads to local displacements and, e.g., originally straight lines are distorted. Smoothing is an effective method to overcome these limitations. However, filtering tends to suppress topographic details. Therefore, multiscale adaptive smoothing is proposed. It flattens if noise is large and relief variation low and smooths a little or not at all where noise is less than the relief [34]. The removal of artificial depressions by filling, breaching, and combining of both is investigated by [35] to support hydrologic applications. Kriging is a statistically sound method for void filling [9]. Other approaches address the removal of striping artifacts caused by the DEM generation process [36], void filling based on an external DEM as a delta surface [33], [37], and vegetation offset correction [36], [38], [39].

Usually, the quality of a DEM is quantified by statistical measures generated by comparing the actual elevation model with a reference model or reference points [26], [40], [41], [42], [43]. In principle, this procedure is suited for the evaluation of edited DEMs, too. Podobnikar [42] uses statistical and visual methods for quality assessment. Statistical approaches are considered to be more objective. Visualizations of the shaded DEM or basic derivatives like slope, aspect, or terrain roughness [44] provide qualitative measures and can balance weaknesses of the statistical methods. Jacobsen [39] and Bayburt *et al.* [45] analyze global DEMs and propose the use of contour lines to assess their morphologic accuracy. However, few approaches focus in detail on the evaluation of artifact improvements in global DEM editing. Some first approaches utilize terrain slopes as indicators for the detection and localization of artificial spikes, stripes, steps, sinkholes, lines, voids (unobserved areas), and coastline effects [46], [47].

Generally, the identification and correction of errors and artifacts in DEMs is done independently of the type of sensor and methodology used for its generation.

In this article, we focus on the improvement of the TanDEM-X DEM compiled by DLR, in particular, on mission-specific and SAR inherent effects. First, we describe the technical approaches used to seamlessly fill data gaps and voids. Next, we explore the detection of the coast lines and inland water bodies by utilizing the SAR coherence, amplitude, and external data. We then present a sophisticated edge-preserving approach for DEM smoothing that is controlled by the height error map (HEM), a quality measure of the TanDEM-X DEM generation process. The quality of the described techniques is finally assessed by a qualitative and quantitative comparison of the TanDEM-X DEM and the resulting edited TanDEM-X DEM. In addition to statistical measures, the latter was supplemented with an assessment of artifacts similar to the approach of Hirt [46].

II. TANDEM-X DEM EDITING

In order to correct the SAR inherent artifacts described in Section I and hence, to enable the full usability of the TanDEM-X DEM, we developed and implemented several editing techniques. To optimize the DEM for a variety of different applications, we considered the following requirements:
1) Infill of other DEM sources at larger data gaps (optional).
2) Water body delineation.
3) Constant water heights at lakes.
4) Consistent heights for oceans.
5) Consistent flow of rivers.
6) Filtering with preservation of break line structures.
7) Smoothing of noisy areas.
8) Interpolation of outliers and invalid areas.

A. Editing Approach

Fig. 1 outlines the framework for the editing processing workflow of TanDEM-X DEM data. It is based on a concept presented in [48] that was continuously enhanced and further developed since then.

The TanDEM-X DEM products consist of the elevation data (DEM) and additional information layers, such as amplitude images (AMP), HEM, and water indication masks (WAM) [21] which we use to identify areas for editing. The AMP provides the mean of all calibrated amplitude values from the contributing DEM scenes. The height error of the HEM is mainly derived from the interferometric coherence and is an excellent indicator for noise. The WAM bases on a threshold method, which evaluates coherence and amplitude values [49].

External information like other existing water masks can be ingested into the system as well. Optionally, it is possible to integrate external DEM datasets where TanDEM-X has larger data gaps.

The sequentially performed editing steps are summarized in four major tasks as follows:
1) DEM infill with other datasets (optional).
2) Flattening of water bodies.
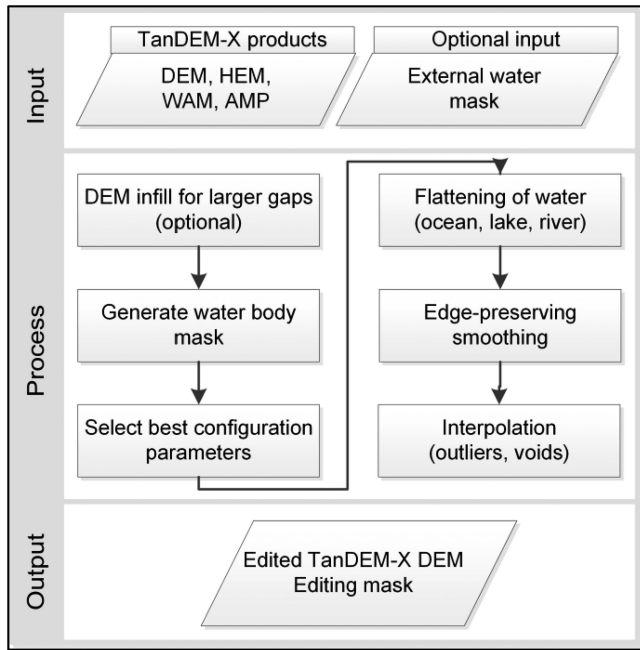3) Edge-preserving smoothing.
4) DEM interpolation.

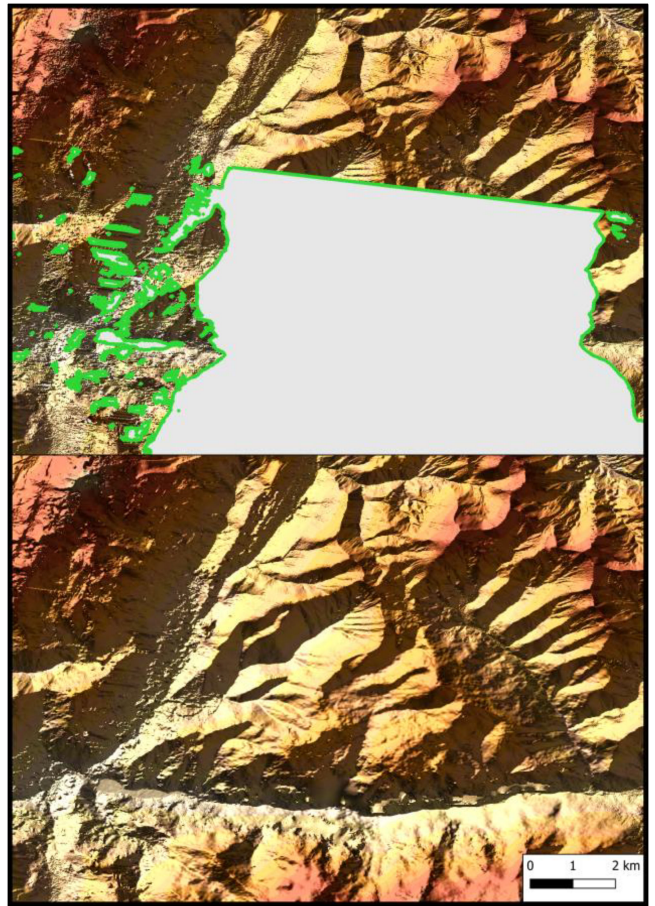Fig. 1. Major steps of the editing framework for TanDEM-X DEMs.

Fig. 2. Tile N45E006 Subset. (Top) TanDEM-X DEM with gap, transition zone between TanDEM-X DEM, and external data superimposed in green. (Bottom) TanDEM-X DEM filled with SRTM-C band data.

B. DEM Infill With Other Datasets

The TanDEM-X DEM has a very high overall coverage of more than 99.8% of the Earth's landmasses [22]. However, larger void areas in the data may still occur for several reasons, e.g., over shadow and layover areas in mountains or due to the lack of input data (some input acquisitions were not acquired or were rejected automatically or interactively during the TanDEM-X DEM generation process due to low return signal power or phase unwrapping errors, etc.). A void interpolation for smaller regions, as proposed in Section II-E-2 (interpolation of void areas), would lead to undefined results for such large invalid areas. Therefore, we employed a procedure for integrating other elevation data into the TanDEM-X DEM.

This procedure is based on a well-established technique to combine multisource DEMs and is utilized for in-house applications, e.g., orthorectification, for many years [50]. This fusion method was further adapted to improve TanDEM-X DEM gap filling with other elevation data such as SRTM and/or ASTER GDEM.

These datasets can be fitted into the TanDEM-X data gaps by considering the TanDEM-X heights within a well-defined boundary around the void areas (Fig. 2, top). Only within this border zone, we fused the TanDEM-X heights with the external dataset by weighted averaging. The weighting is done based on the HEM with an additional feathering of TanDEM-X weights toward its data gap [51]. The feathering effect is calculated within a moving window of 51 square pixels and the local weight for data border handling is given by (1):

$$p = \left[\frac{n - \frac{s^2}{2}}{\frac{s^2}{2}} \right]^2 \text{ for } n > \frac{s^2}{2} \qquad (1)$$

where p is the local weight for border handling, n is the coverage with valid height data, and s is the size of the moving window [51].

The result of an SRTM-C band (1 arcsec) infill is shown in Fig. 2, bottom. Areas filled with external datasets are excluded from the subsequent editing steps.

All elevation models in this article are presented as color shaded relief. In all cases, the illumination source is in the northwest with an elevation of 30°. The heights are exaggerated by the factor five.

Two different colormaps were selected (Fig. 3), one for mountainous areas (Figs. 2, 7, and 8) and one for moderate relief (Figs. 4, 5, 10, 11, and 12).

C. Flattening of Water Bodies

Water bodies in the TanDEM-X DEM are characterized by noisy, random, or invalid values. Therefore, the processing of these areas to achieve a constant height level of the water bodies is necessary for many applications. Initially, we identified water bodies that should be flattened. In this context, a distinction is made between algorithms for inland waters and ocean areas. To detect inland waters, the indication mask (WAM) or any external
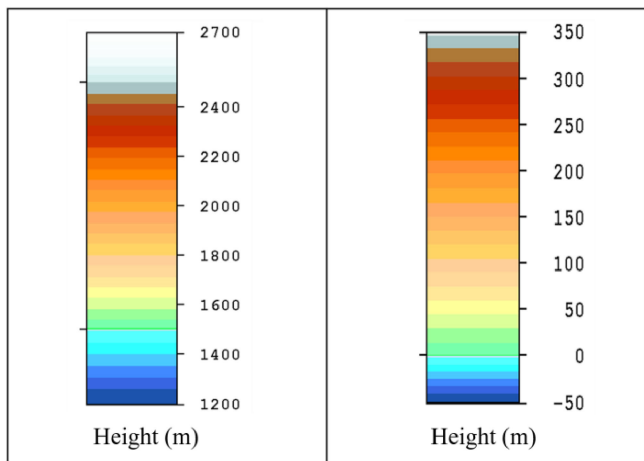
Fig. 3. Colormaps used for the color shaded relief presentations. (Left): colormap for mountainous areas (Figs. 2, 7, and 8). (Right): Colormap for moderate relief (Figs. 4, 5, 10, 11, and 12).

Fig. 5. Tile N13E109 Subset: (a) TanDEM-X DEM; (b) Copernicus DEM 90 ocean flags in blue; (c) refined TanDEM-X ocean flags in blue; (d) TanDEM-X DEM with buffered ocean flags in blue; (e) edited TanDEM-X DEM (smoothed toward geoid heights).
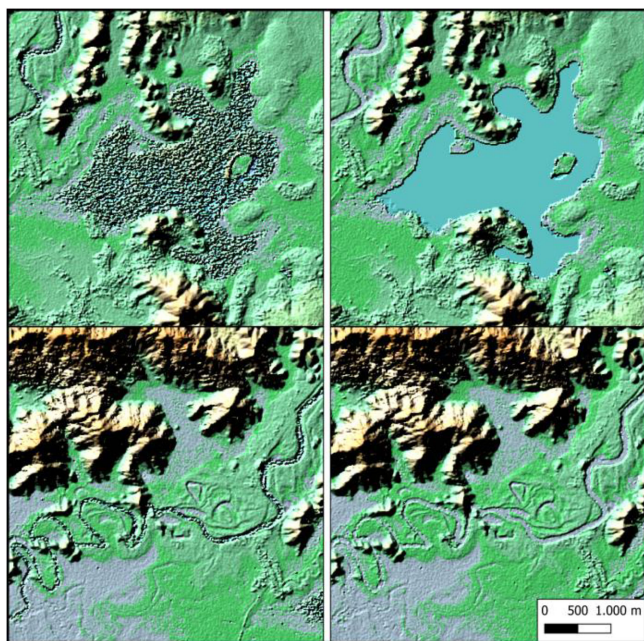

Fig. 4. Tile N12E108 Subset: (top left): lake in TanDEM-X DEM; (top right) lake with constant height in edited TanDEM-X DEM; (bottom left): river in TanDEM-X DEM; (bottom right) river with continuous heights in edited TanDEM-X DEM.
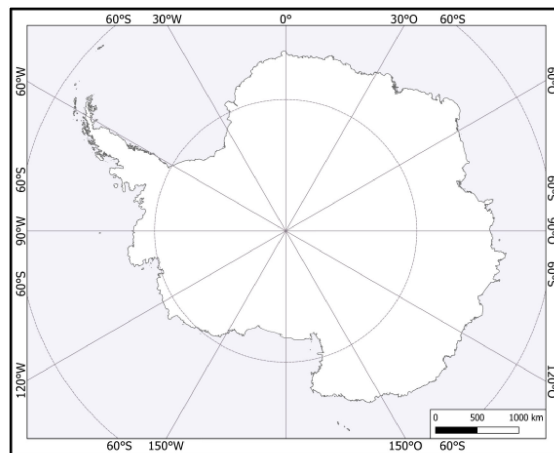
Fig. 6. Vector dataset of the TanDEM-X coastline demarcating open sea areas. It was generated in the course of Antarctica DEM editing.

water mask can be used. Ocean areas can be determined and processed with the help of a coast detection algorithm.

1) Inland Water Body Detection: Compared to external water masks, it is advantageous to use the WAM as it has the same acquisition time and spatial resolution as the TanDEM-X DEM. For DEM processing, we can adapt the WAM interactively by selecting a suitable combination of inherent water flags that represent the probability of water [21]. The quality of the WAM showed reliable results in reference tests [28]. It was demonstrated that regional differences in quality can be found due to land cover and climate zone, and that high quality can

only be guaranteed by a precise and sophisticated selection of classification results. In contrast, external water masks have the disadvantage that they represent different water levels and must be adapted to the TanDEM-X data.

We interactively derived the best suited water mask by selecting the most appropriate combination of water flags from the
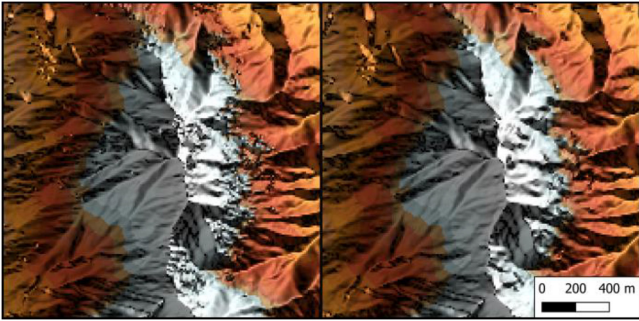
Fig. 7.　(Left) Tile N31E055 Subset: TanDEM-X DEM, (right) Tile N31E055 Subset: smoothed by edge-preserving filtering.
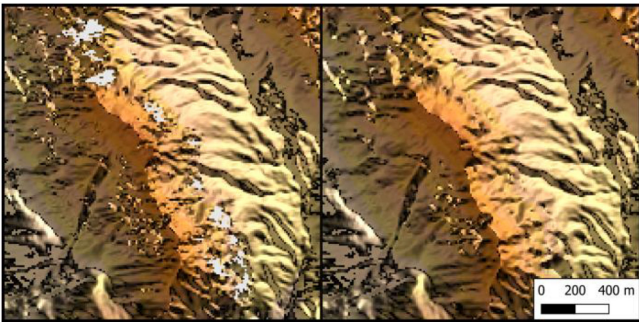
Fig. 8.　(Left) Tile N31E055 Subset: TanDEM-X DEM, (right) Tile N31E055 Subset: voids filled with kriging approach.

WAM. This water mask is subsequently used for the flattening of rivers and lakes. Lakes identified in the water mask obtain a constant height value, which is determined from the elevation values from the lake perimeter. Taking the lowest value of the surrounding elevation values along the lake shore would usually underestimate the actual water level as they are still affected by noise. To account for this noise, we choose the height value of the 20th percentile of all surrounding elevation values, i.e., 20% of the shoreline elevations are below the assigned lake height (Fig. 4, top).

The approach for river flattening is also based on the surrounding elevation values of the river banks. In a joint evaluation of the WAM and the DEM with regard to extent and slope, we identified supporting points along the course of the river, roughly centered in the middle of the stream. For these points, we derived elevations from the surrounding bank heights. A slight but continuous slope along rivers was achieved by interpolation between these nodes leading to more homogeneous elevations as can be seen in Fig. 4, bottom.

2) Coastline Detection: In order to demarcate open sea areas, we derived a coastline based on DEM, AMP, and HEM. Additionally, an external reference coastline was utilized as a starting point.

The algorithm was set up to work with an arbitrary reference dataset [52]. However, due to the recent availability of the Copernicus 90 m DEM [53], which itself is based on the TanDEM-X DEM, the ocean flags of the Copernicus dataset

were used as a proxy. In a first step, the external ocean flags are oversampled to the original resolution, i.e., from Copernicus' 90 m pixel size to the high-resolution 12 m (0.4 arcsec) of TanDEM-X DEM (Fig. 5). Additionally, we can add sea or land areas manually to the water approximation layer where necessary. Prior to processing, we determine a variable set of configuration parameters for each tile, e.g., the AMP, DEM, and HEM thresholds applied in the next step.

As the actual coastline within the 12 m dataset is assumed to be close to the 90 m dataset, a buffer of ca. ± 120 m is set around the approximated coastline. Within this buffer, we define potential land areas if the following three thresholds are jointly fulfilled: the digital numbers (DN) of the AMP layer must be above a threshold of 50 DN to identify brighter land areas, DEM values must be above the threshold of the mean geoid height $+2$ m as we assume land areas to be higher than the mean sea level plus a defined margin, and HEM values must be below 3 m as the height error values are in general lower for land areas than for noisy water areas.

The external coastline serves as a start line and is successively adjusted to the potential land areas by applying erosion and dilation operations. Thereby, we refine the external coastline toward the higher resolution TanDEM-X dataset. With a final erosion and dilation operation, we ensure the removal of small artifacts and the smoothing of the resulting coastline. As the coastline detection is executed tile-based, an automatic correction is executed in order to match detected coastlines of adjacent tiles, as they may show misalignment. The resulting coastline is subsequently used to accurately assign consistent heights for the open sea, around islands and even continents. For that, we utilize geoid heights from the commonly used Earth Gravitational Model 2008 [54]. As the TanDEM-X DEM contains ellipsoidal heights, these geoid heights represent the corresponding mean-sea-level.

To account for possible inaccuracies of the derived coastline, we define another buffer of approximately 120 m starting from the coastline toward the open sea [Fig. 5(c) and (d)]. All elevations within this buffer are assumed to have an elevation in between the last valid land height and the geoid height. Outliers above corresponding land heights are therefore replaced by interpolated heights and outliers below geoid height are replaced with the corresponding geoid height itself. Finally, we combined the resulting TanDEM-X heights of the buffer zone with the corresponding geoid heights by distance weighted averaging. This produces a homogenous transition from land to the open sea elevation as shown in Fig. 5(e).

The first completely edited TanDEM-X DEM is the TanDEM-X Polar DEM 90 [52]. It is based on an updated version of the TanDEM-X DEM for the Antarctic which has integrated some additional acquisitions for gap filling. We separated the ocean areas from the land areas using the coastline detection described above and using the coastline of the Scientific Committee on Antarctic Research from the Antarctic Digital Database as proxy.

Within this process, we created a TanDEM-X coastline vector dataset (Fig. 6) with a total length of 62 971 km, spanning shelf ice as well as land areas.
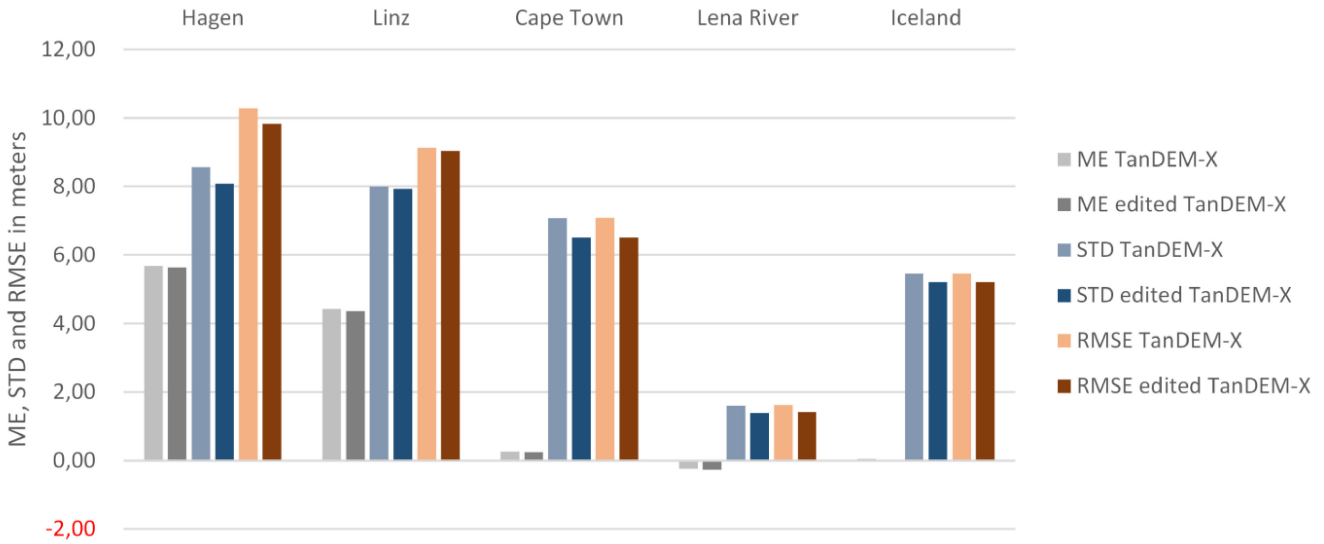
Fig. 9. ME, STD, and RSME of the DEM of differences (TanDEM-X DEM minus reference DEM/edited TanDEM-X DEM minus reference DEM) for the test sites Hagen, Linz, Cape Town, Lena River, and Iceland.
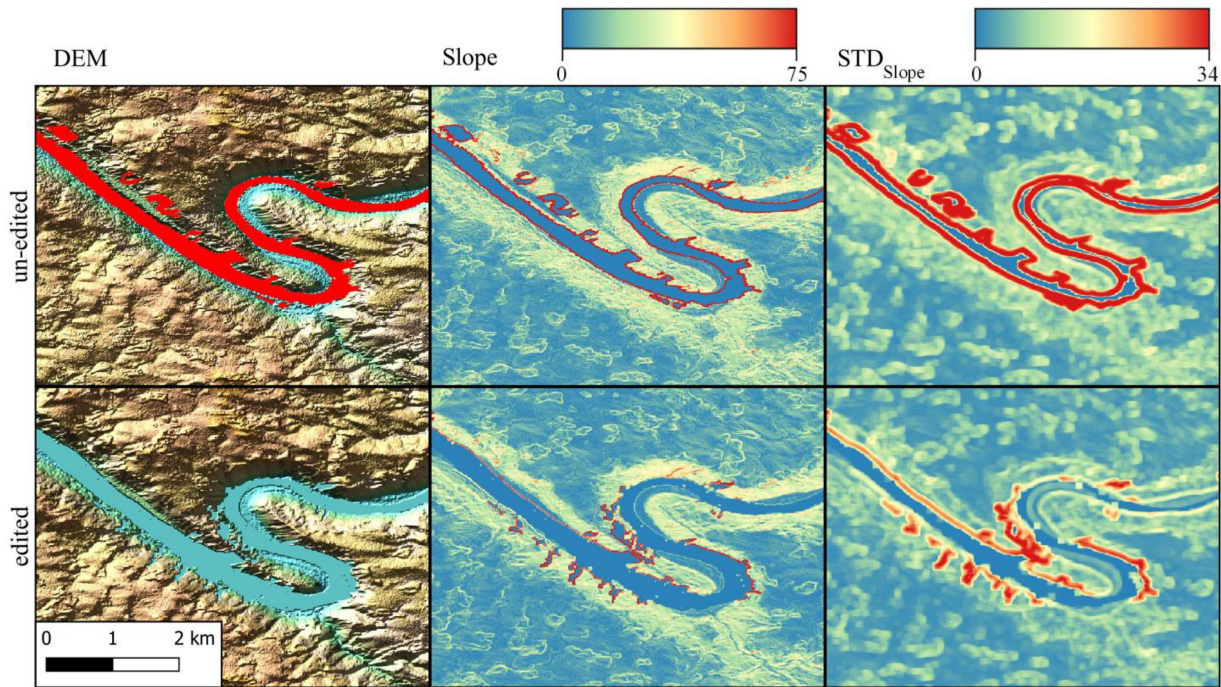
Fig. 10. Tile N48E013, Passau: TanDEM-X DEM with larger void areas (depicted red in the shaded DEM) and the corresponding edited DEM.

D. Edge Preserving Smoothing

For smoothing, we applied an inverse HEM weighted filter which considers edge preservation in order to maintain break line structures, like dikes and levees which are important for flood modeling as well as ridges and peaks for orthorectification.

For nonedge pixels, we ensured this by considering only pixels for filtering which are located at distances smaller than the closest detected edge in the DEM, e.g., a ridge. Filtering across edges would otherwise result in elevations being systematically too low (across ridges) or too high (across troughs). Edge pixels on the other hand are filtered by considering only pixels of the corresponding edge being within the given filtering radius. Again, this avoids that heights are underestimated (ridges) or overestimated (troughs), respectively.

1) Edge Detection: The result of the edge detection approach is based on analyzing curvatures in the DEM. For noise reduction in the elevation data, we smoothed the elevation values

Fig. 11.   Tile N48E013, Passau: TanDEM-X DEM with void areas (depicted red in the shaded DEM) and the corresponding void filled DEM.

Fig. 12.   Tile N48E013, Passau: TanDEM-X DEM with void areas (depicted red in the shaded DEM) and the corresponding edited DEM with erroneous water identification effects.

before computing the curvature. We considered a 3×3 boxcar filter to be sufficient. This filtering is only done temporarily for edge detection. The filtered values are not sto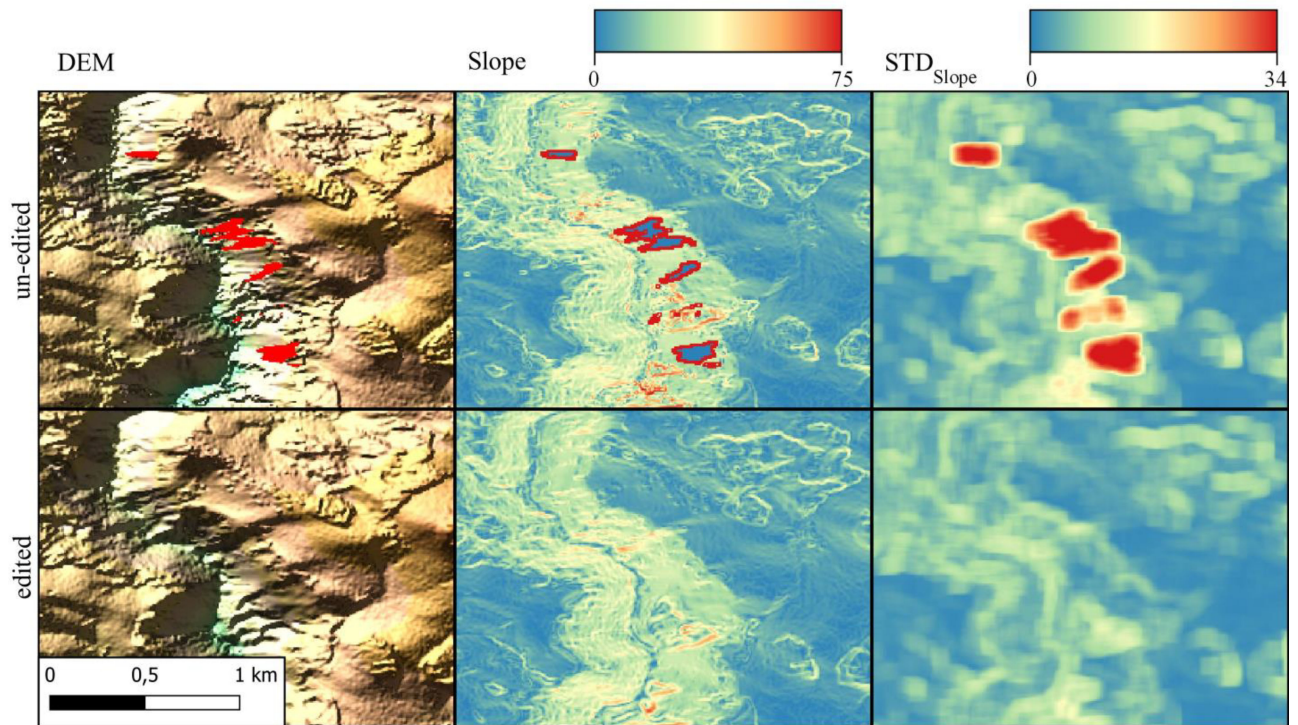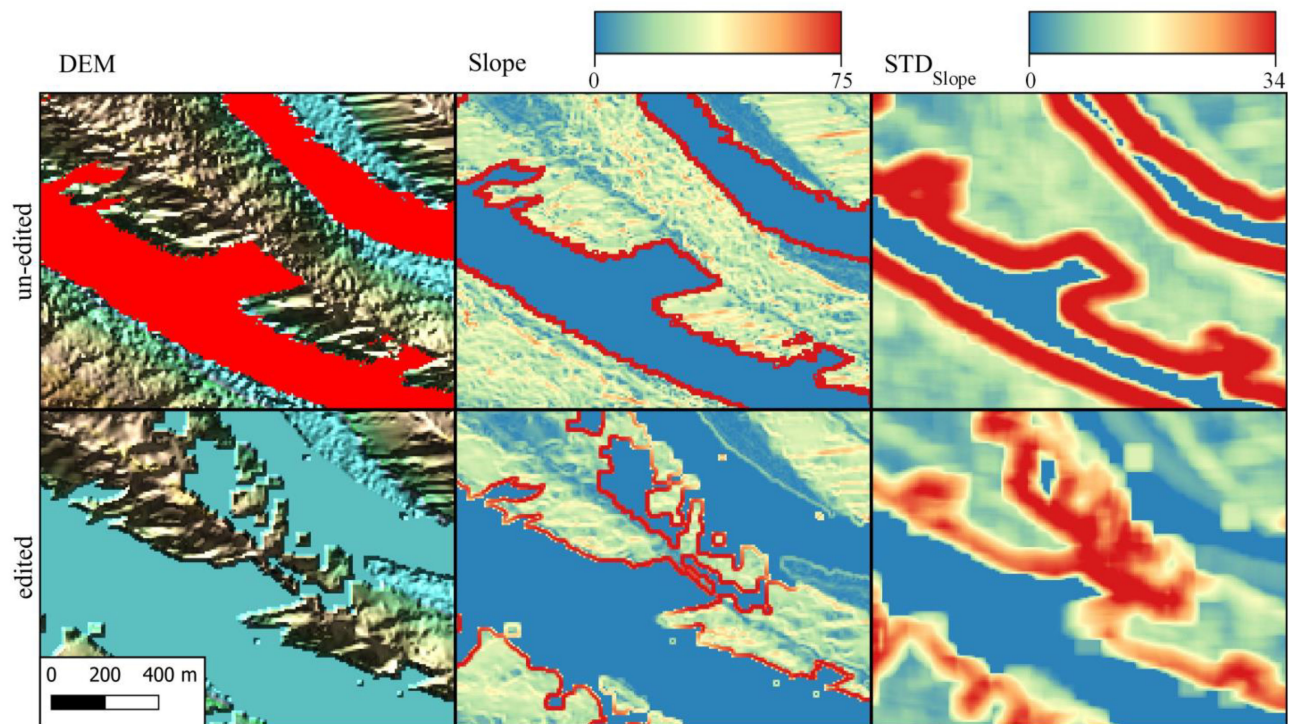red. A pixel is considered as part of an edge if the calculated curvature in an arbitrary direction within a configurable window (e.g., 5×5 pixels) exceeds a given threshold. Finally, we grouped the edge pixels into regions. Regions (i.e., contiguous edges) consisting of fewer than a defined number of pixels are not considered.

2) Edge-Preserving DEM Filter Algorithm: Large areas within the TanDEM-X DEM already provide a reliable and smooth representation of the Earth's surface due to the processing strategy of combining at least two or more acquisitions [55]. However, noisy pixels still remain because of unfavorable acquisition geometries (e.g., slopes) or a limited number of acquisitions. These noisy elevation values are indicated by an increased HEM value. We only smooth pixels if corresponding HEM values exceed a predefined threshold. Thus, the original TanDEM-X values are preserved where appropriate (Fig. 7). The degree of smoothing is defined by a configurable filter radius. In order to avoid averaging across topographic edges, this filter radius is adapted for nonedge pixels in case of nearby edges. In this case, the applied filter radius is reduced to be smaller than the closest edge pixel. The smoothing itself is performed by replacing the elevation pixel with an HEM weighted average of its neighborhood values. The weights applied are inversely proportional to the corresponding values of the HEM, meaning pixels with higher height errors have less impact on the final elevation value. Note that we also filter edge pixels with this approach, but only those pixels belonging to the same continuous edge and located within the filter radius are included in the averaging.

E. DEM Interpolation

Besides larger gaps which we can fill with external datasets as described in Section II-B (DEM infill with other datasets), even smaller void areas or single void pixels may occur. We interpolate these voids based on the surrounding valid values. In addition, an interpolation for single outliers may be required.

1) Detection and Interpolation of Outliers: Single outlier pixels are defined relative to their local statistics. The local median value is computed within a circular region of a given radius centered on each pixel. If this median value is outside a certain confidence interval around the pixel value itself, we consider the value as an outlier. Unlike smoothing, the new elevation value is solely interpolated from the surrounding pixels and the original value is not considered. Additionally, minimum and maximum thresholds are introduced to avoid improper results. By this, we ensure that independently of the confidence interval, all deviations greater than the maximum threshold are flagged as outliers. Similarly, no deviations less than the minimum outlier threshold are flagged.

2) Interpolation of Void Areas: Smaller void areas mainly occur due to low return signal or shadow and layover effects. Depending on the complexity of the terrain, the interpolation should not exceed the area of a few square kilometers to avoid undefined interpolation artefacts. We estimate the elevations

within these void areas from a subset of adjacent valid pixels. The subset of the surrounding pixels used for the interpolation of each individual pixel is determined pixel-by-pixel. First, we group all pixels on the selected perimeter into a predefined number of direction bins of equal angular width. Within each of these bins, a predefined number of pixels closest to the pixel to be interpolated is selected. The elevation of this point is then estimated from this subset (2):

$$h_0 = \sum_{i=0}^{N-1} \lambda_i h_i. \tag{2}$$

In (2) h_i are the elevations from which the interpolated elevation h_0 is estimated and λ_i are the weights. We determine these weights by kriging [56]. While a simple inverse distance weighting for example only considers distances, kriging accounts for the spatial covariance between the surrounding pixels. These covariance values can be determined by empirical variograms or variogram models. While empirical variograms have the advantage of being estimated from the data itself, their properties do not always satisfy the conditions to be valid for kriging. Variogram models on the other hand are always valid and serve as an approximation of the empirical variograms. The most common models are the spherical, exponential, and Gaussian variogram models. We apply the Gaussian model (3) to determine the covariance values in our workflow:

$$\gamma(d) = n + (s-n) * \left(1 - e^{-\frac{3d^2}{r^2}}\right) \text{ for } d > 0. \tag{3}$$

In this function, n is defined the nugget—i.e., the *y*-intercept of the variogram—which represents noise. The parameter s is the sill value, which is the maximum value that the variogram tends toward at infinity, the parameter r is range, which is the distance at which the variogram levels out and values are no longer correlated, and the parameter d is the distance between elevation values.

We then use these covariance values to estimate the void pixel's elevation from the subset of surrounding pixels (Fig. 8).

III. QUALITY ASSESSMENT

A. Quality Assessment Methods

In Section II, several editing tasks and their qualitative improvement of the TanDEM-X DEM have been presented. By utilizing shaded representations of the corresponding DEMs, the benefit for different applications were illustrated. Besides this qualitative assessment by visual methods, the improvements can also be shown by quantitative measurements as presented in the following.

1) Quantitative Accuracy Assessment: The quality of a DEM can be quantified by statistical measures, derived from a model-to-model comparison of the TanDEM-X DEM and a reference DEM [26]. The reference DEM h_{ref} is hereby subtracted from the corresponding TanDEM-X pixel h_i:

$$\Delta h = h_i - h_{ref}. \tag{4}$$

We can obtain the distribution of the errors from a histogram. Assuming a normal distribution, the following statistical measures are applied to assess the error in more detail:

Mean error (ME)

$$ME = \frac{1}{n}\sum_{i=1}^{n} h_i - h_{\text{ref}} = \frac{1}{n}\sum_{i=1}^{n}\Delta h_i. \qquad (5)$$

Root mean square error (RMSE)

$$RMSE = \sqrt{\frac{1}{n}\sum_{i=1}^{n}\Delta h_i{}^2}. \qquad (6)$$

Error standard deviation (STD)

$$STD = \sqrt{\frac{1}{n-1}\sum_{i=1}^{n}(\Delta h_i - ME)^2}. \qquad (7)$$

In case of non-normal error distribution, further accuracy measures are required as proposed by [57]:

Median (50% quantile)

$$\hat{Q}_{\Delta h}(0.5) = m_{\Delta h}. \qquad (8)$$

Median absolute deviation (MAD)

$$MAD = \text{median}_j\left(|\Delta h_j - m_{\Delta h}|\right). \qquad (9)$$

Normalized median absolute deviation (NMAD)

$$NMAD = 1.4826 \cdot \text{median}_j\left(|\Delta h_j - m_{\Delta h}|\right) \qquad (10)$$

and the absolute deviation at the 90% quantile, also known as the LE90

$$\hat{Q}_{|\Delta h|}(0.9). \qquad (11)$$

We assess the improvements achieved by the DEM editing by comparing the statistical measures of (5)–(11) determined by subtracting reference models from the edited and the original version of the TanDEM-X DEM. The NMAD is proportional to the median of the absolute differences and can be regarded as an estimate for the error standard deviation (STD) without considering larger outliers [57]. We expect that the smoothing as well as the removal of outliers and noisy water bodies of the DEM editing will lower these statistical measures and therewith reflect the improvement.

2) Assessment of Artifacts: Artifacts can originate from, e.g., incomplete or erroneous processing, both during the DEM generation and the subsequent editing. However, their presence cannot be derived reliably solely from the statistics. Hirt [46] proposes the maximum slope approach for the analysis of the 90 m DEMs of SRTM and MERIT (multierror-removed improved terrain). A threshold of 5 m/m (~78°) was applied to distinguish natural slopes from artificial terrain features. In total, 1341 artifacts were detected in the entire SRTM dataset and 108 in MERIT. In our case, we want to assess the editing quality of the TanDEM-X DEM, which is provided in a much higher spatial resolution of 12 m. Consequently, it has to be considered that the threshold is not only sensitive to artifacts, but also to natural and man-made features due to the higher level of detail. The

edges of high forest stands, dams, poles, and towers can lead to significant changes in altitude from one pixel to the next and they can cause high slopes as well. Therefore, the maximum slope and the standard deviation of the slope (STD_{Slope}) are jointly employed. The STD_{Slope} is sensitive to abrupt changes and discontinuities in the slope. It identifies steep smooth slopes and rough surface areas. Furthermore, the STD_{Slope} tends to enhance noise and errors in the original DEM [44]. The standard deviation of the slope is calculated using an 11×11 moving window. The slope itself was determined from the vicinity of 3 $\times$ 3 pixels around every DEM pixel.

3) Data: The quantitative and the qualitative accuracy assessments are applied to DEM geocells (tiles) with dimensions of 1° by 1° for both the TanDEM-X data and its edited version. The corresponding test sites represent different types of relief and land cover and require the application of the different DEM editing techniques.

Reference DEMs are available for five sites enabling a model-to-model accuracy assessment. They were derived from airborne laser scanning (LIDAR = LIght Detection And Ranging) or from high-resolution optical satellite data (ArcticDEM [58]). LIDAR enables the determination of the terrain height (DTM = digital terrain model), while the ArcticDEM provides the surface height (DSM = digital surface model). Geographic names of the different test sites, the corresponding data source of the reference DEMs, and their characteristics are listed in Table I. We calculate the statistics of the TanDEM-X DEM considering only pixels having valid values in the reference and the TanDEM-X DEM itself. The statistics of the edited DEM were calculated in the same way. Voids in either one of the DEM datasets are not considered.

Slope and STD_{Slope} are calculated for nine tiles for the assessment of artifacts that are listed in Table II; again, for both the TanDEM-X DEM and its edited version. In addition to the five sites of the model-to-model comparison, we included four further DEM tiles into the assessment of artifacts to broaden the number of samples and test cases.

B. Quality Assessment Results

1) Model-to-Model Accuracy Assessment: The results of the statistical measures which we derived by subtracting a reference DEM from both the TanDEM-X DEM and from the edited TanDEM-X DEM are shown in Fig. 9 and listed in more detail in Table A.I in the appendix for the five different test sites.

Common to all sites is that the MEs remain almost unchanged during the editing process (Fig. 9): *Cape Town* (0.26 vs. 0.24 m), *Lena River* (−0.24 vs. −0.27 m), *Iceland* (0.04 vs. −0.01 m). They differ only by a few centimeters. Whereas, the ME is higher for the sites *Hagen* (5.68 vs. 5.64 m) and *Linz* (4.42 vs. 4.36 m). In these two cases, the reference DEM is a terrain model obtained by airborne LIDAR, while TanDEM-X provides the height of the surface. The higher ME is caused by the land cover like forests and built-up areas. The reference DEM of the *Cape Town* site is a terrain model as well. However, this site is characterized by low vegetation like bushland and lower, sparse forest resulting in low ME values as stated above.

TABLE I
HIGH RESOLUTION REFERENCE DEMs USED FOR QUANTITATIVE ACCURACY ASSESSMENT

Site	Data source	Period of acquisition	Pixel spacing	Height range (WGS84)	Elevation type	Terrain characteristics
Hagen, Germany	LIDAR	2013 - 2019	5 m	52 m to 711 m	DTM	Urban, rural, moderate relief
Linz, Austria	LIDAR	2015 - 2020	10 m	268 m to 1,423 m	DTM	Moderate relief, forest, grassland, urban
Cape Town, South Africa	LIDAR	2011-2015	10 m	–4 m to 1,621 m	DTM	Flat, table mountain, low vegetation
Lena River, Siberia	ArcticDEM (optical)	2012 - 2017	10 m	-16 m to 371 m	DSM	Flat, tundra, cliffs
Iceland	ArcticDEM (optical)	2010 - 2017	10 m	-58 m to 1,738 m	DSM	Glaciers, volcanos, mountains

TABLE II
TanDEM-X DEM TILES USED FOR ARTIFACT ASSESSMENT

Site	TanDEM-X product tile ID	Height range (WGS84)	Terrain characteristics	Editing characteristics
Hagen, Germany	TDM1_DEM__04_N51E007_DEM	24 m to 727 m	Urban, rural, moderate relief	Water bodies, outliers, smoothing
Passau, Germany	TDM1_DEM__04_N48E013_DEM	196 m to 1,496 m	Moderate relief, forest,	Voids, edge preserving filtering
Linz, Austria	TDM1_DEM__04_N48E014_DEM	172 m to 1,284 m	grassland, urban	
Cape Town, South Africa	TDM1_DEM__04_S34E018_DEM	-126 m to 1,621 m	Urban, flat, table mountain,	Coast, voids, outliers, smoothing
	TDM1_DEM__04_S35E018_DEM	-336 m to 1,531 m	low vegetation	
Lena River, Siberia	TDM1_DEM__04_N72E126_DEM	-57 m to 371 m	Flat, tundra, cliffs	Edge preserving smoothing, voids
Iceland	TDM1_DEM__04_N64W022_DEM	66 m to 1,736 m	Glacier, volcanos, mountains	Coast, water bodies, smoothing
Albertville, France	TDM1_DEM__04_N45E006_DEM	269 m to 4,841 m	Alpine terrain, glaciers, steep slopes	Voids, gaps, edge preserving filtering
Vietnam	TDM1_DEM__04_N12E108_DEM	2 m to 2,429 m	Flat, mountainous, reservoirs, low and dense vegetation	Water bodies, small rivers, smoothing

TABLE III
ARTIFACTS IN TanDEM-X DEM

Site	TanDEM-X product tile ID	Slope >78°	No. of pixels	SD$_{Slope}$>34°	No. of pixels
Hagen, Germany	TDM1_DEM__04_N51E007_DEM	4	395	2	610
Passau, Germany and Austria	TDM1_DEM__04_ N48E013 _DEM	58	47,474	36	96,837
Linz, Austria	TDM1_DEM__04_ N48E014 _DEM	4	540	0	0
Cape Town I, South Africa	TDM1_DEM__04_ E018S33 _DEM	8	380,473	3	503,462
Cape Town II, South Africa	TDM1_DEM__04_ E018S34 _DEM	15	1,310,931	5	2,566,440
Lena River, Siberia	TDM1_DEM__04_N72E126_DEM	0	0	0	0
Iceland	TDM1_DEM__04_N64W022_DEM	2	304	0	0
Albertville, France	TDM1_DEM__04_N45E006_DEM	317	468,365	189	279,892
Vietnam	TDM1_DEM__04_N12E108_DEM	2	313	0	0

The reduction of the STD and the RMSE values in Fig. 9 reflect the smoothing effects of the filtering and the flattening of water bodies during the editing process. The STD could be lowered by several decimeters between 0.21 m (*Lena Delta*) and 0.58 m (*Cape Town*). The RMSE values behave very similarly, decreasing by 0.20 m (*Lena Delta*) and 0.59 m (*Cape Town*). The purpose of the filtering is the reduction of noise, while preserving terrain details at the same time.

ME, STD, RMSE, as well as maximum and minimum values of the *Lena River Delta* site are significantly smaller compared to the other sites. Here, TanDEM-X measured the area during

winter, when all water bodies are frozen. Very few pixels displayed open water conditions causing noise that was removed during the editing.

All LE90 values are reduced by the editing process: *Cape Town* (2.46 vs. 2.34 m), *Lena River* (1.64 vs. 1.61 m), *Iceland* (2.88 vs. 2.69 m), *Hagen* (19.75 vs. 19.10 m), and *Linz* (18.14 vs. 17.78 m). The latter two are significantly higher as the reference DEMs are DTMs and the scenes represent larger urban resp. forested, hilly areas that causes larger differences.

It is noticeable that minimum and maximum errors are almost in the same range after the editing as before. One reason is

TABLE IV
ARTIFACTS IN EDITED TANDEM-X DEM

Site	TanDEM-X product tile ID	Slope >78°	No. of pixels	SD_{Slope}>34°	No. of pixels
Hagen, Germany	TDM1_DEM__04_N51E007_DEM	0	0	0	0
Passau, Germany and Austria	TDM1_DEM__04_N48E013_DEM	43	5,424	30	5,367
Linz, Austria	TDM1_DEM__04_N48E014_DEM	0	8	0	0
Cape Town I, South Africa	TDM1_DEM__04_E018S33_DEM	2	129	0	0
Cape Town II, South Africa	TDM1_DEM__04_E018S34_DEM	15	4,986	8	3,256
Lena River, Siberia	TDM1_DEM__04_N72E126_DEM	0	0	0	0
Iceland	TDM1_DEM__04_N64W022_DEM	0	0	0	0
Albertville, France	TDM1_DEM__04_N45E006_DEM	49	56,871	15	1,733
Vietnam	TDM1_DEM__04_N12E108_DEM	0	27	0	25

that the reference DEMs are provided in an unedited version and still contain voids and noise values. Positive values mean that the TanDEM-X DEM is higher than the reference model. The TanDEM-X DEM is the source for the maximum and the minimum deviations at three sites. The differences result from disadvantageous interactions of steep slopes and low coherence. The *Cape Town* site shows the highest differences. Here, a valley was not detected in the interferometric DEM and the TanDEM-X DEM is consequently much higher than the reference. In contrast, an incorrectly derived mountain ridge causes the TanDEM-X DEM being lower than the reference. Both effects are the result of a phase unwrapping error. The minimum and maximum values are slightly improved by the smoothing during the editing process but the phase unwrapping error was not corrected. The interaction of larger void area in the Danube River, relief, and low coherence are the reason for the extreme difference values of the *Linz* DEMs after the editing by overestimating a slope and by erroneously extending a water surface into the adjacent flank of a hill. Temporal changes between the acquisition of TanDEM-X and the reference DEM lead to the minimum and maximum values of the Hagen site. No significant improvement of the values for MAD and NMAD could be observed (Table A.I). As these are more robust measures, they do not reflect the removal of noise, even for larger noise areas, like the ocean in the *Cape Town* site, the values remain almost unchanged with and without editing.

To highlight the improvement especially in more noisy areas, two separate lines per site and editing status were added in Table A.I, showing the influence of height errors lesser and higher than 1 m. An annotated height error below 1 m means almost noise-free conditions. Consequently, the statistical parameters are nearly unaffected by the editing while those of noisier values with a height error greater than 1 m are clearly improved.

2) Assessment of Artifacts: Next, we assess the presence and numbers of artifacts per DEM tile, based on the slope and the standard deviation of the slope. The criteria are slopes reaching and exceeding an angle of 78° as well as a threshold of 34° with respect to the STD_{Slope}. Additionally, these criteria must be fulfilled for at least 20 adjacent pixels. The results are provided in Table III for the TanDEM-X DEM tiles and Table IV for the corresponding edited version. For every site and threshold, the number of artifacts and the corresponding number of pixels are listed.

The proposed method is sensitive to four different types of artifacts as follows:
1) Voids including data gaps (missing acquisitions).
2) Edges caused by the DEM processing.
3) Extreme slopes indicating the presence of phase unwrapping problems.
4) Noise.

Only the *Lena River* DEM showed no artifacts in the original version. In all other tiles—except the *Albertville* DEM tile which will be treated separately—up to 58 features were detected while considering the slope and up to 36 when applying the 34° threshold to the STD_{slope}. The number of pixels per site showing a slope value higher than 78° varies between 304 and more than 1.3 million. In three cases, the STD_{slope} did not exceed the threshold of 34°, even though the slope indicates the presence of two and four artifacts, respectively. As the STD_{slope} is calculated from a pixel's vicinity, the number of pixels affected by an artifact is generally higher than the one of the slope. The two *Cape Town* DEM tiles show a relatively low number of artifacts in relation to the high number of pixels being affected. Both *Cape Town* DEM tiles cover land and ocean. The high number of pixels is caused by a long borderline between meaningful values mainly over land and voids and extreme noise over open water areas. Fig. 10 shows a similar effect of an elongated void area in the Danube River in the *Passau* DEM tile. The void area is clearly visible in the slope and the STD_{slope} images.

The editing significantly reduced the number of affected height values in all test sites and even removed all artifacts for four of the test sites. Fig. 11 shows the filling of smaller void areas. They are clearly visible in the DEM, the slope, and the STD_{slope} images. No voids and therewith no artifacts are visible after the editing process. Fig. 12 is an example where the artifact could just partially be corrected. After the editing, the void area in the Danube River that previously consisted of one object is now split into several disconnected components. Accordingly, the number of artifacts in the edited tile *Passau* is still relatively high.

In very few cases, new artifacts were introduced by the editing. In particular, incomplete or erroneous identification of water-covered areas can lead to a false flattening where real terrain should be present. Islands and depressions can also remain where a flattened water surface would be correct. In total, five such cases were detected; three in the *Cape Town* tiles, one in the *Passau* tile, and one in the *Linz* DEM tile.

The *Albertville* DEM is located in the Alps and is characterized by rough terrain with steep slopes, glaciers, and snow-covered areas. Consequently, more areas fulfill the 78° slope criterion and more potential artifacts are detected. Additionally, more voids appear due to low backscatter or layover and shadow effects and the site even suffers from a data gap caused by a missing acquisition (Fig. 2). The high numbers of artifacts and affected pixels reflect these conditions in Table III. However, a comparison with Table IV highlights the improvement achieved by the editing. The number of artifacts and corresponding pixels is significantly lower.

All artifacts could be completely removed in the DEM tiles *Hagen, Linz, Iceland*, and *Vietnam*.

IV. DISCUSSION

The introduced semi-automatic procedure for editing the TanDEM-X DEM mainly focuses on the removal of data gaps, voids, and noisy water covered areas. Additionally, we reduce system inherent random noise in the DEM while terrain details are preserved at the same time. The flattening of water bodies, the edge-preserving smoothing, and the interpolation of outliers and voids is done automatically based on given configuration parameters. Furthermore, we can manually adapt the generation of the water mask and the coastline as well as the optional DEM infill to achieve the best possible results for individual high-resolution DEM tiles.

In particular, the editing of water bodies strongly depends on the water delineation quality. Areas showing low coherence and backscatter values but which are not part of a river nor a lake can falsely be treated as water bodies. Such conditions appear if, e.g., steep slopes causing radar shadow are close to water bodies, wet snow, or dry sand are present or forest and topography interact in an unfavorable way. Consequently, the corresponding area is filled with a constant height and an artificial lake is created in the edited DEM where relief should be present. The operator-assisted selection of the water body classification was introduced in order to minimize false water body delineations. The quality assessment results highlight the improvements achieved by this procedure. Nevertheless, limits in the water body detection exist.

Another issue of the water delineation is the water level. The presented approach considers the situation at the time of the TanDEM-X mapping. If several acquisitions exist, the lowest water level is considered. A requirement of a specific level like high or low tide is not fulfilled. For hydrologic applications, specific river levels are generally not important, provided a continuous flow direction can be ensured. The algorithm we developed for continuous height estimation represents a high potential for the application of flood scenarios, as the actual water surface is found more effectively.

Edge preserving smoothing refines and improves the feature identification (e.g., clearings). The statistical measures demonstrate the smoothing effect. The STDs of the quantitative analysis of all sites could be reduced between 1% for the *Linz* DEM tile and 13% at the *Lena Delta*. As requested, the smoothing is stronger in areas showing a higher noise level (HEM > 1 m). Here, the STD reduction varies between 9% (*Cape Town*) and 22% (*Lena Delta*).

The assessment of artifacts is a quite new topic in quantifying global DEM data [46]. Also, the new technique to use the slope and the STD_{Slope} complemented the detection of erroneous areas. This approach is in particular recommendable for high spatial resolution DEMs. It could be shown that edges caused by the DEM processing, voids, and data gaps were successfully detected by these measures. This represents a step forward to quantifying DEM editing improvements by comparing the artifacts before and after editing. Unfortunately, the goal to detect phase unwrapping errors did not work reliably with the slope and STD_{Slope} technique. Usually, phase unwrapping errors occur in highly undulated terrain. Steep slopes and break lines are created by false phase unwrapping. At the same time, the natural shape of the terrain looks very similar and the error cannot reliably be distinguished. Nevertheless, significant deviations can be detected by comparison with an external reference DEM. Areas affected by phase unwrapping errors can then be masked out and filled using the DEM infill procedure described in Section II–B.

As a side-effect of this article, the TanDEM-X DEM was evaluated for five test sites. Wessel *et al.* [26] reported that the TanDEM-X DEM exceeds the 10 m (90%) performance goal, often by factors up to 5. Three of the five test sites support this trend. The LE90 values of *Cape Town* (2.46 vs. 2.34 m), *Lena River* (1.64 vs. 1.61 m), and *Iceland* (2.88 vs. 2.69 m) are well within the performance goal. Two sites do not meet the 90% requirement of 10 m. The LE90 values for *Hagen* (19.75 vs. 19.10 m) and *Linz* (18.68 vs. 18.37 m) are significantly higher. However, in these cases, the differences result from comparing a surface model (TanDEM-X DEM) with a terrain model (Table I). Nevertheless, the LE90 is in all cases lower after the editing.

V. CONCLUSION

We have presented a semi-automated editing workflow for full resolution 0.4" TanDEM-X DEM data. The quality analysis has revealed the weaknesses but also the strengths of this semi-automatic process. The editing of rivers and lakes indicated a clear potential for improvement, this approach is currently being further developed by using machine learning and we expect to complete it in the near future. Nevertheless, the editing steps (DEM infill, DEM interpolation, and edge-preserving) showed high quality processing in both visual and statistical terms.

The first complete edited product, the TanDEM-X Polar DEM 90 for the Antarctica, proved to find a high use in the scientific community. The next steps will be the editing of Iceland, Greenland, and North America.

APPENDIX

ACCURACY NUMBERS (M) FOR TANDEM-X DEM AND EDITED TANDEM-X DEM VERSUS HIGH RESOLUTION REFERENCE DEM WITH TWO HEIGHT ERROR
CLASSES FROM TANDEM-X HEIGHT ERROR MAP (HEM) - BOLD FIGURES INDICATE TOTAL NUMBERS OF THE ENTIRE TESTSITE

Height error (m)	No. of pixels	ME (m)	STD (m)	RMSE (m)	MAD (m)	NMAD (m)	LE90 (m)	Max. error (m)	Min. error (m)	No. of voids
Hagen, Germany										
TanDEM-X										
HEM 0 - 1.0	23,332,793	4.00	7.47	8.47	1.54	2.28	17.56	122.43	-91.80	0
HEM > 1.0	7,922,904	10.64	9.63	14.35	6.83	10.12	22.81	151.14	-130.97	0
Whole area	**31,255,697**	**5.68**	**8.57**	**10.28**	**2.81**	**4.17**	**19.75**	**151.14**	**-130.97**	**236**
edited TanDEM-X										
HEM 0 - 1.0	23,332,793	4.00	7.46	8.46	1.54	2.29	17.54	119.79	-91.80	0
HEM > 1.0	7,922,904	10.48	7.80	13.06	5.82	8.62	21.18	114.62	-87.89	0
Whole area	**31,255,933**	**5.64**	**8.05**	**9.83**	**2. 66**	**3.95**	**19.10**	**119.79**	**-91.80**	**0**
Linz, Austria										
TanDEM-X										
HEM 0 - 1.0	81,141,180	3.41	7.16	7.93	0.70	1.04	16.23	84.84	-226.49	0
HEM > 1.0	11,767,874	11.43	9.71	14.99	6.61	9.90	23.00	228.58	-245.60	0
Whole area	**92,909,054**	**4.42**	**7.99**	**9.13**	**0.97**	**1.44**	**18.14**	**228.58**	**-245.60**	**116,88 0**
edited TanDEM-X										
HEM 0 - 1.0	81,141,180	3.40	7.15	7.92	0.70	1.04	16.20	83.82	-232.01	0
HEM > 1.0	11,767,874	11.02	8.85	14.13	6.06	8.99	21.53	**144.57**	-248.91	0
Whole area	**93,025,934**	**4.36**	**7.93**	**9.04**	**0.98**	**1.46**	**17.78**	**144.57**	**-255.52**	**0**
Cape Town, South Africa (coastal waters masked)										
TanDEM-X										
HEM 0 - 1.0	16,316,679	0.20	2.78	2.78	0.58	0.86	1.89	140.34	-282.17	0
HEM > 1.0	1,083,870	1.16	26.24	26.27	3.84	5.69	25.80	368.36	-495.23	0
Whole area	**17,400,549**	**0.26**	**7.08**	**7.09**	**0.62**	**0.92**	**2.46**	**368.36**	**-495.23**	**13,273**
edited TanDEM-X										
HEM 0 - 1.0	16,316,679	0.19	2.77	2.78	0.58	0.86	1.89	136.66	-268.53	0
HEM > 1.0	1,083,870	1.05	23.63	23.65	2.76	4.09	22.02	359.71	-479.76	0
Whole area	**17,413,822**	**0.24**	**6.50**	**6.50**	**0.62**	**0.92**	**2.34**	**359.71**	**-479.76**	**0**
Lena River, Siberia										
TanDEM-X										
HEM 0 - 1.0	35,314,950	-0.29	1.08	1.12	0.56	0.82	1.59	63.29	-116.65	0
HEM > 1.0	1,042,749	1.59	6.82	7.00	1.16	1.72	10.51	63.42	-143.28	0
Whole area	**36,357,699**	**-0.24**	**1.60**	**1.62**	**0.56**	**0.84**	**1.64**	**63.42**	**-143.28**	**0**
edited TanDEM-X										
HEM 0 - 1.0	35,314,950	-0.30	1.07	1.11	0.56	0.83	1.59	63.29	-116.65	0
HEM > 1.0	1,042,749	0.64	5.29	5.33	0.70	1.04	3.49	60.07	-140.66	0
Whole area	**36,357,699**	**-0.27**	**1.39**	**1.42**	**0.56**	**0.83**	**1.61**	**63.29**	**-140.66**	**0**
Iceland (coastal waters masked)										
TanDEM-X										
HEM 0 - 1.0	75,697,410	0.08	3.93	3.93	0.67	1.00	2.52	379.79	-424.52	0
HEM > 1.0	2,524,353	-0.88	21.40	21.42	6.02	8.93	20.67	229.93	-404.22	0
Whole area	**78,221,763**	**0.04**	**5.46**	**5.46**	**0.70**	**1.04**	**2.88**	**379.79**	**-424.52**	**0**
edited TanDEM-X										
HEM 0 - 1.0	75,697,410	0.05	3.98	3.98	0.67	1.00	2.52	379.79	-424.52	0
HEM > 1.0	2,524,353	-1.81	18.97	19.06	1.49	2.21	15.78	175.77	-415.36	0
Whole area	**78,221,763**	**-0.01**	**5.20**	**5.20**	**0.69**	**1.02**	**2.69**	**379.79**	**-424.52**	**0**

REFERENCES

[1] L. Hawker, J. Neal, and P. Bates, "Accuracy assessment of the TanDEM-X 90 digital elevation model for selected floodplain sites," *Remote Sens. Environ.*, vol. 232, 2019, Art. no. 111319.

[2] R. Tavares da Costa, P. Mazzoli, and S. Bagli, "Limitations posed by free DEMs in watershed studies: The case of river Tanaro in Italy," *Frontiers Earth Sci.*, vol. 7, no. 141, pp. 1–15, 2019.

[3] V. Lecours, R. Devillers, E. N. Edinger, C. J. Brown, and V. L. Lucieer, "Influence of artefacts in marine digital terrain models on habitat maps and species distribution models: A multiscale assessment," *Remote Sens. Ecol. Conserv.*, vol. 3, no. 4, pp. 232–246, 2017.

[4] R. Sørensen and J. Seibert, "Effects of DEM resolution on the calculation of topographical indices: TWI and its components," *J. Hydrol.*, vol. 347, no. 1–2, pp. 79–89, 2007.

[5] S. P. Wechsler, "Uncertainties associated with digital elevation models for hydrologic applications: A review," *Hydrol. Earth Syst. Sci.*, vol. 11, no. 4, pp. 1481–1500, 2007.

[6] T. Ullmann, C. Büdel, and R. Baumhauer, "Characterization of arctic surface morphology by means of intermediated TanDEM-X digital elevation model data," *Zeitschrift für Geomorphologie*, vol. 61, no. 1, pp. 3–25, 2017.

[7] P. Grosse, B. van Wyk de Vries, P. A. Euillades, M. Kervyn, and I. A. Petrinovic, "Systematic morphometric characterization of volcanic edifices using digital elevation models," *Geomorphology*, vol. 136, no. 1, pp. 114–131, 2012.

[8] R. J. Pike, I. S. Evans, and T. Hengl, "Geomorphometry: A brief guide," in *Developments in Soil Science*, vol. 33, T. Hengl and H. Reuter, Eds. Amsterdam, The Netherlands: Elsevier, 2009, pp. 3–30.

[9] H. I. Reuter, T. Hengl, P. Gessler, and P. Soille, "Preparation of DEMs for geomorphometric analysis," in *Developments in Soil Science*, vol. 33, T. Hengl and H. Reuter, Eds. Amsterdam, The Netherlands: Elsevier, 2009, pp. 87–120.

[10] H. J. Persson, H. Olsson, M. J. Soja, L. M. H. Ulander, and J. E. S. Fransson, "Experiences from large-scale forest mapping of Sweden using TanDEM-X data," *Remote Sens.*, vol. 9, no. 12, 2017, Art. no. 1253.

[11] M. Schlund, F. von Poncet, S. Kuntz, H. D. V. Boehm, D. H. Hoekman, and C. Schmullius, "TanDEM-X elevation model data for canopy height and aboveground biomass retrieval in a tropical peat swamp forest," *Int. J. Remote Sens.*, vol. 37, no. 21, pp. 5021–5044, 2016.

[12] M. Simard, N. Pinto, J. B. Fisher, and A. Baccini, "Mapping forest canopy height globally with spaceborne lidar," *J. Geophys. Res.*, vol. 116, no. 4, 2011, Art. no. G04021.

[13] E. Meier, U. Frei, and D. Nuesch, "Precise terrain corrected geocoded images," in *SAR Geocoding: Data and Systems*, G. Schreier, Ed. Karlsruhe, Germany: Herbert Wichmann Verlag GmbH, 1993, pp. 173–185.

[14] D. Small, "Flattening gamma: Radiometric terrain correction for SAR imagery," *IEEE Trans. Geosci. Remote Sens.*, vol. 49, no. 8, pp. 3081–3093, Aug. 2011.

[15] C. Tucker, D. Grant, and J. Dykstra, "NASA's global orthorectified landsat data set," *Photogramm. Eng. Remote Sens.*, vol. 55, pp. 378–390, 2003.

[16] T. Toutin, "State-of-the-art of geometric correction of remote sensing data: A data fusion perspective," *Int. J. Image Data Fusion*, vol. 2, pp. 3–35, 2011.

[17] C. Ressel and N. Pfeifer, "Evaluation of the elevation model influence on the orthorectification of sentinel-2 satellite images over austria," *Eur. J. Remote Sens.*, vol. 51, pp. 693–709, 2017.

[18] B. Purinton and B. Bookhagen, "Validation of digital elevation models (DEMs) and comparison of geomorphic metrics on the southern central andean plateau," *Earth Surf. Dyn.*, vol. 5, pp. 211–237, 2017.

[19] J. Collins, G. Riegler, H. Schrader, and M. Tinz, "Applying terrain and hydrological editing to TanDEM-X data to create a consumer-ready World-DEM product," *Int. Arch. Photogramm. Remote Sens. Spatial Inf. Sci.*, vol. 40, no. 7, pp. 1149–1154, 2015.

[20] M. Zink *et al.*, "TanDEM-X: The new global DEM takes shape," *IEEE Geosci. Remote Sens. Mag.*, vol. 2, no. 2, pp. 8–23, Jun. 2014.

[21] B. Wessel, "TanDEM-X ground segment – DEM products specification document," EOC, DLR, Oberpfaffenhofen, Germany, Public Document TD-GSPS-0021, Issue 3.2, 2018. Accessed: Jul. 14, 2020. [Online]. Available: https://tandemx-science.dlr.de/

[22] P. Rizzoli *et al.*, "Generation and performance assessment of the global TanDEM-X digital elevation model," *ISPRS J. Photogramm. Remote Sens.*, vol. 132, pp. 119–139, 2017.

[23] A. Gruber, B. Wessel, M. Huber, and A. Roth, "Operational TanDEM-X DEM calibration and first validation results," *ISPRS J. Photogramm. Remote Sens.*, vol. 73, pp. 39–49, 2012.

[24] H. Zwally *et al.*, "ICESat's laser measurements of polar ice, atmosphere, ocean, and land," *J. Geodyn.*, vol. 34, no. 3–4, pp. 405–445, 2002.

[25] M. Huber *et al.*, "Ensuring globally the TanDEM-X height accuracy: Analysis of the reference data sets ICESat, SRTM, and KGPS-Tracks," in *Proc. IEEE Int. Geosci. Remote Sens. Symp.*, 2009, pp. II–769–II–772.

[26] B. Wessel, M. Huber, C. Wohlfart, U. Marschalk, D. Kosmann, and A. Roth. "Accuracy assessment of the global TanDEM-X digital elevation model with GPS data," *ISPRS J. Photogramm. Remote Sens.*, vol. 139, pp. 171–182, 2018.

[27] R. Bamler and P. Hartl "Synthetic aperture radar interferometry," *Inverse Problems*, vol. 10, no. 4, pp. R1–R54, 1998.

[28] A. Wendleder, B. Wessel, A. Roth, M. Breunig, K. Martin, and S. Wagenbrenner, "TanDEM-X water indication mask: Generation and first evaluation results," *IEEE J. Sel. Topics Appl. Earth Observ. Remote Sens.*, vol. 6, no. 1, pp. 171–179, Feb. 2013.

[29] S. Suchandt, M. Eineder, H. Breit, and H. Runge, "Analysis of ground moving objects using SRTM/X-SAR data," *ISPRS J. Photogramm. Remote Sens.*, vol. 61, no. 3–4, pp. 209–224, 2006.

[30] H. A. Zebker and J. Villasenor, "Decorrelation in interferometric radar echoes," *IEEE Trans. Geosci. Remote Sens.*, vol. 30, no. 5, pp. 950–959, Sep. 1992.

[31] M. Martone, P. Rizzoli, and G. Krieger, "Volume decorrelation effects in TanDEM-X interferometric SAR data," *IEEE Geosci. Remote Sens. Lett.*, vol. 13, no. 12, pp. 1812–1816, Dec. 2016.

[32] J. Slater *et al.*, "The SRTM data 'finishing' process and products," *Photogramm. Eng. Remote Sens.*, vol. 72, no. 3, pp. 237–247, 2006.

[33] J. Takaku, T. Tadono, M. Doutsu, F. Ohgushi, and H. Kai, "Updates of 'AW3D30' ALOS global digital elevation model with other open access datasets," *Int. Arch. Photogramm. Remote Sens. Spatial Inf. Sci.*, vol. XLIII-B4-2020, pp. 183–189, 2020.

[34] J. C. Gallant, "Adaptive smoothing for noisy DEMs," in *Proc. Geomorphmetry*, 2011, pp. 37–40.

[35] J. B. Lindsay and I. F. Creed, "Removal of artifact depressions from digital elevation models: Towards a minimum impact approach," *Hydrol. Process.*, vol. 19, no. 16, pp. 3113–3126, 2005.

[36] J. C. Gallant, "Enhancing the SRTM data for Australia," in *Proc. Geomorphmetry*, 2009, pp. 149–154.

[37] G. Grohman, G. Kroenung, and J. Strebeck, "Filling SRTM voids: The delta surface fill method," *Photogramm. Eng. Remote Sens.*, vol. 72, no. 3, pp. 213–216, 2006.

[38] J. C. Gallant, A. M. Read, and T. I. Dowling, "Removal of tree offsets from SRTM and other digital surface models," *Int. Arch. Photogramm. Remote Sens. Spatial Inf. Sci.*, vol. 39, no. 4, pp. 275–280, 2012.

[39] K. Jacobsen, "Characteristics and accuracy of large area covering height models," *Int. Arch. Photogramm. Remote Sens. Spatial Inf. Sci.*, vol. 40, no. 1W1, pp. 157–162, 2013.

[40] K. Jacobsen, "Development of large area covering height model," *Int. Arch. Photogramm. Remote Sens. Spatial Inf. Sci.*, vol. 40, no. 4, pp. 105–110, 2014.

[41] U. Soergel, K. Jacobsen, and L. Schack, "TanDEM-X mission: Overview and evaluation of intermediate results," *Int. Arch. Photogramm. Remote Sens. Spatial Inf. Sci.*, vol. 40, no. 7W2, pp. 225–230, 2013.

[42] T. Podobnikar, "Methods for visual quality assessment of a digital terrain model," *Sapiens*, vol. 2, no. 2, 2009. Accessed: Jun. 29, 2020. [Online]. Available: http://journals.openedition.org/sapiens/738

[43] P. F. Fisher and N. J. Tate, "Causes and consequences of error in digital elevation models," *Prog. Phys. Geogr.*, vol. 30, no. 4, pp. 467–489, 2006.

[44] C. Grohmann, M. Smith, and C. Riccomini, "Multiscale analysis of topographic surface roughness in the midland valley, scotland," *IEEE Trans. Geosci. Remote Sens.*, vol. 49, no. 4, pp. 1200–1213, Apr. 2011.

[45] S. Bayburt, A. B. Kurtak, G. Büyüksalih, and K. Jacobsen, "Geometric accuracy analysis of WorldDEM in relation to AW3D30, SRTM and ASTER GDEM2," *Int. Arch. Photogramm. Remote Sens. Spatial Inf. Sci.*, vol. 42, no. 1W1, pp. 211–217, 2017.

[46] C. Hirt, "Artefact detection in global digital elevation models (DEMs): The maximum slope approach and its application for complete screening of the SRTM v4.1 and MERIT DEMs," *Remote Sens. Environ.*, vol. 207, pp. 27–41, 2018.

[47] D. G. Brown and T. J. Bara, "Recognition and reduction of systematic error in elevation and derivative surfaces from 7 1/2-minute DEMs," *Photogramm. Eng. Remote Sens.*, vol. 60, no. 2, pp. 189–194, 1994.

[48] M. Huber, B. Wessel, A. Wendleder, J. Hoffmann, and A. Roth, "A framework for an automatical editing of TanDEM-X digital elevation models," in *Proc. Int. Geosci. Remote Sens. Symp.*, 2015, pp. 3826–3829.

[49] A. Wendleder, M. Breunig, K. Martin, B. Wessel, and A. Roth, "Water body detection from TanDEM-X data: Concept and first evaluation of an accurate water indication mask," in *Proc. IEEE Int. Geosci. Remote Sens. Symp.*, 2011, Art. no. 4.

[50] A. Roth, W. Knöpfle, G. Strunz, M. Lehner, and P. Reinartz, "Towards a global elevation product: Combination of multi-source digital elevation models," *Int. Arch. Photogramm. Remote Sens. Spatial Inf. Sci.*, vol. 34, no. 4, 2002. Accessed: Jul. 29, 2020. [Online]. Available: https://www.isprs.org/proceedings/XXXIV/part4/pdfpapers/210.pdf

[51] W. Knöpfle, G. Strunz, and A. Roth, "Mosaicking of digital elevation models derived by SAR interferometry," *Int. Arch. Photogramm. Remote Sens. Spatial Inf. Sci.*, vol. 32, no. 4, 1998. Accessed: Jul. 29, 2020. [Online]. Available: https://www.isprs.org/proceedings/XXXII/part4/knoepfle108.pdf

[52] The TanDEM-X PolarDEM project, DLR – Earth Observation Center. Accessed: Sep. 16, 2020. [Online]. Available: https://www.dlr.de/eoc/en/desktopdefault.aspx/tabid-11882/20871_read-66374

[53] Copernicus DEM - ESA. Accessed: Sep. 23, 2020. [Online]. Available: https://spacedata.copernicus.eu/web/cscda/data-offer/core-datasets

[54] EGM2008 Development Team: EGM2008 - WGS 84 Version, 2012. [Online]. Available: https://earth-info.nga.mil/GandG/wgs84/gravitymod/egm2008/egm08_wgs84.html

[55] A. Gruber, B. Wessel, M. Martone, and A. Roth, "The TanDEM-X DEM mosaicking: Fusion of multiple acquisitions using InSAR quality parameters," *IEEE J. Sel. Topics Appl. Earth Observ. Remote Sens.*, vol. 9, no. 3, pp. 1047–1057, Mar. 2016.

[56] C. Deutsch and A. Journel, *GSLIB – Geostatistical Software Library and User's Guide*. New York, NY, USA: Oxford Univ. Press, 1992.

[57] J. Höhle and M. Höhle, "Accuracy assessment of digital elevation models by means of robust statistical methods," *ISPRS J. Photogramm. Remote Sens.*, vol. 64, no. 4, pp. 398–406, 2009.

[58] The ArcticDEM initiative. Accessed: May 11, 2021. [Online]. Available: https://www.pgc.umn.edu/data/arcticdem/

Martin Huber received the engineering degree (Dipl.-Ing.) in geodesy from the Technical University Munich, Munich, Germany, in 2002.

He joined the German Aerospace Centre (DLR) as a Researcher with the German Remote Sensing Data Center (DFD), in 2002. He has expertise in radar image processing, with focus on orthorectification and image analysis. Within the TanDEM-X mission, he is part of the "Mosaicking and Calibration Processor" development team, which is accountable for the final TanDEM-X DEM generation. Furthermore, he is responsible for the maintenance and development of the Digital Elevation Model Database (DEM-DB) at the DFD. The DEM-DB supports storage, extraction, and fusion of DEMs with different resolution and quality. His research interests include SAR image processing, digital elevation models, and hydrological topics.

Nicole Osterkamp received the M.Sc. degree in geography with a focus on geomatics from Ruhr-University Bochum, Bochum, Germany, in 2019.

She did her master thesis in collaboration with the German Remote Sensing Data Center (DFD), German Aerospace Center (DLR), Weßling, Germany. She is currently working as a Research Associate with the Company for Remote Sensing and Environmental Research (SLU), Munich, Germany. Her research interests include the development of SAR-based geoinformation products with focus on cryosphere and hydrological topics.

Ursula Marschalk received the engineering degree (Dipl.-Ing. FH) in cartography from the University of Applied Sciences Munich, Munich, Germany, in 1991.

In 1990, she started working with the German Aerospace Centre (DLR) at the Devision for Planetary Research as a Head of the Regional Planetary Image Facility. She joined DLR's German Remote Sensing Data Center (DFD), in 1991, where she was involved in the implementation and operation of a SAR geocoding system for the ERS- and X-SAR-missions. Her research interests include digital elevation models from SAR data for several missions (ERS-1/2, SRTM/X-SAR, and TanDEM-X).

Raphael Tubbesing received the M.Sc. degree in applied physical geography and mountain research from the Karl-Franzens-University Graz, Graz, Austria, in 2020.

His thesis has been done in collaboration with the German Remote Sensing Data Center (DFD), German Aerospace Center (DLR), Weßling, Germany. Thematically, he dealt with machine learning and deep learning in the context of building extractions for hazard susceptibility estimation. He is currently working as a Research Associate with the company for Remote Sensing and Environmental Research (SLU), Munich, Germany. His research interests include dynamics of the earth's surface and the coupling with the atmosphere, especially in cold and polar regions.

Anna Wendleder received the university degree (Dipl.-Ing.) in geodesy and geoinformation from the Technical University of Munich, Munich, Germany, in 2008, with the thesis "Exemplary Generation and Analyses of Digital Elevation Models generated by simulated TanDEM-X acquisitions."

She is currently a Scientific Researcher with the German Remote Sensing Data Center, German Aerospace Center. She was involved in the mosaicking, calibration, and validation of the global TanDEM-X digital elevation model and the generation of the TanDEM-X water indication mask. She is currently responsible for the orthorectification of SAR data and build-up the multi-SAR system, a framework for the processing, orthorectification, and polarimetric decomposition of all available SAR data to analysis ready data. Her research interests include mapping of snow cover extent, monitoring of snow-covered sea ice processes, and derivation of snow depth based on the copolar phase difference based on SAR data.

Birgit Wessel received the diploma degree in geodesy from the University of Hanover, Hanover, Germany, in 2000, and the Doctor of Engineering degree (Dr.-Ing.) in geodesy from the Technische Universitt Mnchen (TUM), Munich, Germany, in 2006.

From 2000 to 2005, she was a Scientific Collaborator with the Institute for Photogrammetry and Cartography, TUM. Since 2005, she has been with the German Remote Sensing Data Center, German Aerospace Center (DLR), where she currently is leading the DEM calibration and mosaicking developments for the German interferometric TanDEM-X satellite mission. Her research interests include SAR remote sensing and InSAR DEMs.

Achim Roth received the engineering degree (Dipl.-Ing.) in geodesy from the University of Karlsruhe, Karlsruhe, Germany, in 1987.

He joined the German Aerospace Centre (DLR), in 1987, for the development and implementation of an operational SAR-geocoding system for the ERS- and X-SAR-missions. Since 1991, he has been leading the team "SAR Topography" at DLR's German Remote Sensing Data Center (DFD). From 2000 to 2004, he was the SRTM/X-SAR Ground Segment Manager. Since 2002, he has been the TerraSAR-X Science Coordinator. It contributed to the Shuttle Radar Topography Mission and is currently involved in the TerraSAR-X and TanDEM-X missions. His research interests include development of geoinformation products from SAR data, the corresponding retrieval techniques, and their implementation as operational processors.